Endoplasmic reticulum chaperones stabilize ligand-receptive MR1 molecules for efficient presentation of metabolite antigens

Hamish E. G. McWilliam[a,b,1,2], Jeffrey Y. W. Mak[c,d,1], Wael Awad[e,f], Matthew Zorkau[a], Sebastian Cruz-Gomez[a], Hui Jing Lim[a], Yuting Yan[a], Sam Wormald[g,h], Laura F. Dagley[g,h], Sidonia B. G. Eckle[a], Alexandra J. Corbett[a], Haiyin Liu[b], Shihan Li[a,i], Scott J. J. Reddiex[a,i,j], Justine D. Mintern[b], Ligong Liu[c,d], James McCluskey[a], Jamie Rossjohn[e,f,k], David P. Fairlie[c,d,2], and Jose A. Villadangos[a,b,2]

[a]Department of Microbiology and Immunology, The University of Melbourne, The Peter Doherty Institute for Infection and Immunity, Melbourne, VIC 3000, Australia; [b]Department of Biochemistry and Molecular Biology, The University of Melbourne, Bio21 Molecular Science and Biotechnology Institute, Parkville, VIC 3010, Australia; [c]Division of Chemistry and Structural Biology, Institute for Molecular Bioscience, The University of Queensland, Brisbane, QLD 4072, Australia; [d]Australian Research Council Centre of Excellence in Advanced Molecular Imaging, The University of Queensland, Brisbane, QLD 4072, Australia; [e]Infection and Immunity Program, Department of Biochemistry and Molecular Biology, Biomedicine Discovery Institute, Monash University, Clayton, VIC 3800, Australia; [f]Australian Research Council Centre of Excellence in Advanced Molecular Imaging, Monash University, Clayton, VIC 3800, Australia; [g]Division of Systems Biology and Personalised Medicine, The Walter and Eliza Hall Institute of Medical Research, Parkville, VIC 3052, Australia; [h]Department of Medical Biology, University of Melbourne, Parkville, VIC 3010, Australia; [i]Australian Research Council Centre of Excellence in Advanced Molecular Imaging, University of Melbourne, Parkville, VIC 3010, Australia; [j]Murdoch Children's Research Institute, Royal Children's Hospital, Parkville, VIC 3052, Australia; and [k]Institute of Infection and Immunity, Cardiff University School of Medicine, Heath Park, CF14 4XN Cardiff, United Kingdom

Edited by Peter Cresswell, Yale University, New Haven, CT, and approved August 21, 2020 (received for review June 18, 2020)

The antigen-presenting molecule MR1 (MHC class I-related protein 1) presents metabolite antigens derived from microbial vitamin B_2 synthesis to activate mucosal-associated invariant T (MAIT) cells. Key aspects of this evolutionarily conserved pathway remain uncharacterized, including where MR1 acquires ligands and what accessory proteins assist ligand binding. We answer these questions by using a fluorophore-labeled stable MR1 antigen analog, a conformation-specific MR1 mAb, proteomic analysis, and a genome-wide CRISPR/Cas9 library screen. We show that the endoplasmic reticulum (ER) contains a pool of two unliganded MR1 conformers stabilized via interactions with chaperones tapasin and tapasin-related protein. This pool is the primary source of MR1 molecules for the presentation of exogenous metabolite antigens to MAIT cells. Deletion of these chaperones reduces the ER-resident MR1 pool and hampers antigen presentation and MAIT cell activation. The MR1 antigen-presentation pathway thus co-opts ER chaperones to fulfill its unique ability to present exogenous metabolite antigens captured within the ER.

MHC class I-related protein 1 (MR1) | MAIT cells | protein trafficking | fluorescent probe | vitamin B

A critical event in the initiation of adaptive immunity is the presentation of diverse peptide antigens (Ag) by classic major histocompatibility complex (MHC) molecules to conventional T cells, triggering their activation over several days. In contrast, some MHC-like molecules present unique types of Ag to innate-like T cells. These Ag lack the vast diversity of peptide Ag and are chemically distinct, such as lipid Ag presented by the CD1 family, but rapidly activate T cells specific for each MHC-like molecule, kick-starting mechanisms of defense against infection (1).

The least understood, yet most evolutionarily conserved Ag-presentation function is performed by MHC class I-related protein 1 (MR1) (2). MR1 captures and presents exogenous microbial metabolites derived from vitamin B_2 biosynthesis or vitamin B_9 degradation, termed vitamin B-related antigens (VitBAg) (3, 4). The most potent VitBAg known is 5-(2-oxopropylideneamino)-6-D-ribitylaminouracil (5-OP-RU) (4, 5). Since vitamin B_2 is made by many bacteria and fungi but not mammals (6), the presence of VitBAg is an important signature of microbial metabolism (7). When MR1–VitBAg complexes are displayed on the surface of antigen-presenting cells, they are recognized by one of the most abundant types of T cell in humans, the innate-like mucosal-associated invariant T (MAIT) cells (8). Such recognition activates MAIT cells, which release inflammatory cytokines that combat microbial infections and promote tissue repair (9, 10). Furthermore, MR1 may present tumor-specific Ag to MR1-restricted T cells for immunosurveillance of cancer (11, 12).

MAIT cell development, expansion, and T cell receptor (TCR)-mediated activation is dependent on MR1 presentation

Significance

A newly discovered system for immunological detection of diverse bacterial and fungal pathogens involves the MHC-like host protein called MR1. This molecule scavenges metabolites from the biosynthesis of riboflavin by microbes. MR1 presents these compounds on the surface of antigen-presenting cells, where they interact with T cells known as mucosal-associated invariant T cells and stimulate immunity. Critical aspects of the cell biology of metabolite presentation by MR1 are unknown. Here we generated a fluorescent antigen analog and use it to show that MR1 captures its metabolites within the endoplasmic reticulum. We describe proteins that maintain MR1 ready for metabolite binding in the endoplasmic reticulum to promote efficient pathogen detection. MR1 thus monitors extracellular microbial metabolites from within the cell.

Author contributions: H.E.G.M., J.Y.W.M., J.D.M., L.L., J.M., J.R., D.P.F., and J.A.V. designed research; H.E.G.M., J.Y.W.M., W.A., M.Z., S.C.-G., H.J.L., Y.Y., L.F.D., S.B.G.E., A.J.C., S.L., and S.J.J.R. performed research; H.E.G.M., J.Y.W.M., L.L., and D.P.F. contributed new reagents/analytic tools; H.E.G.M., J.Y.W.M., H.J.L., S.W., L.F.D., S.B.G.E., A.J.C., H.L., D.P.F., and J.A.V. analyzed data; and H.E.G.M., J.Y.W.M., D.P.F., and J.A.V. wrote the paper.

Competing interest statement: A.J.C., L.L., S.B.G.E., J.M., J.R., and D.P.F. are named inventors on a patent application (PCT/AU2013/000742, WO2014005194), and J.Y.W.M., L.L., S.B.G.E., A.J.C., J.M., J.R., and D.P.F. are named inventors on another patent application (PCT/AU2015/050148, WO2015149130) involving MR1 ligands for MR1-restricted mucosal-associated invariant T cells, owned by University of Queensland, Monash University, and University of Melbourne.

This article is a PNAS Direct Submission.

[1]H.E.G.M. and J.Y.W.M. contributed equally to this work.

[2]To whom correspondence may be addressed. Email: hamish.mcwilliam@unimelb.edu.au, d.fairlie@imb.uq.edu.au, or j.villadangos@unimelb.edu.au.

This article contains supporting information online at https://www.pnas.org/lookup/suppl/doi:10.1073/pnas.2011260117/-/DCSupplemental.

First published September 21, 2020.

of metabolites produced and secreted by commensal flora (8, 13). Such extracellular metabolites also play critical roles in MAIT cell homeostasis and function in the periphery (10). Thus, deciphering the MR1 presentation pathway for these metabolites is crucial to understanding immunological functions mediated by the MR1–MAIT cell axis. Given the unique nature of VitBAg, it is likely that MR1 presentation involves mechanisms distinct from those engaged in other Ag-presentation pathways. In previous work (14) we demonstrated one such difference: While other human MHC and MHC-like Ag presentation molecules constitutively bind self-ligands within the endoplasmic reticulum (ER) shortly after their synthesis (e.g., endogenous peptides for MHC-I, invariant chain [Ii] for MHC-II or self-lipids for CD1), MR1 lacks such ligands. Instead MR1 accumulates inside the ER in a ligand-receptive conformation with very low levels of MR1 expressed on the cell surface (15–17). Previously, we suggested that extracellular VitBAg reaches ER-resident MR1 via an unknown route, where it forms a covalent bond with a lysine residue (K43) in the MR1 Ag-binding cleft (14). This appeared to trigger a conformational change in MR1 that enabled its recruitment to the cell surface (14). This system prevents MR1 surface expression when not occupied, but facilitates MR1 presentation when its K43 positive charge is neutralized by binding to an Ag. Ligand binding via Schiff base formation is akin to a pathogen-driven posttranslational modification of MR1, a feature absent in other MHC molecules (7).

While the evidence supporting this "ER-loading" model of MR1 presentation is compelling, no direct demonstration of VitBAg binding to ER-resident MR1 molecules has been made. Other studies have suggested that MR1 first leaves the ER and traffics to endosomal compartments to capture VitBAg (18–20). Furthermore, given that all MHC molecules are inherently unstable in the absence of ligands, the presence of "empty" MR1 molecules within the ER implies their stabilization by unknown chaperones. Clarifying the contribution of ER loading to MR1 biology and identifying accessory molecules that enable this mechanism would provide new insights into the mechanisms of VitBAg presentation by MR1 to MAIT cells.

Here we report a fluorescent, epitope-tagged, synthetic compound that closely mimics VitBAg as a tool for tracking the cellular location of MR1-ligand binding. We also show a conformation-specific mAb that defines two distinct ligand-free MR1 conformers, and use unbiased proteomic and genome-wide CRISPR/Cas9 screens to define chaperones that stabilize empty MR1 molecules for efficient VitBAg capture. Our results provide a unique perspective on MR1 molecular interactions and conformational changes in the ER that allow efficient presentation of microbial metabolites to MAIT cells.

Results

Development of a Synthetic, Epitope-Tagged, Fluorescent MR1 Ligand. MR1 ligand 5-OP-RU (compound **9**) (Fig. 1) is generated through a reaction between microbial riboflavin biosynthetic precursor 5-amino-6-D-ribitylaminouracil (5-A-RU) and bacterial or mammalian metabolite methylglyoxal (4). 5-OP-RU is weakly fluorescent with different absorbance and emission spectra to its precursors (*SI Appendix*, Fig. S1*A*) and detectable in cells by flow cytometry (*SI Appendix*, Fig. S1*B*). Its fluorescence increased over time when incubated with C1R cells at 37 °C (*SI Appendix*, Fig. S1*B*) but not at 4 °C (*SI Appendix*, Fig. S1*C*), suggesting that it does not penetrate cell membranes by passive transport. Simultaneously, MR1 expression increased on the cell surface, consistent with 5-OP-RU binding to intracellular MR1 followed by transport to and accumulation at the plasma membrane (*SI Appendix*, Fig. S1*B*) (14). Slightly more 5-OP-RU accumulated in WT C1R cells than in MR1-deficient cells (C1RΔMR1) and even more in C1R cells overexpressing MR1 (C1R.MR1) (*SI Appendix*, Fig. S1*B*). MR1-bound 5-OP-RU is protected from degradation in and export from the cell, in agreement with rapid loss of 5-OP-RU fluorescence but stabilization of surface MR1 expression upon ligand removal from culture medium (*SI Appendix*, Fig. S1*B*). There is no antibody against 5-OP-RU to monitor its localization.

To increase the chemical stability and fluorescence, we developed the epitope-tagged derivative Ag, MR1 Ag analog-tetramethylrhodamine (MAgA-TAMRA; compound **8**) (Fig. 1*A* and *SI Appendix*, *Supplementary Materials and Methods*). A crystal structure (4) for the ternary complex MAIT TCR-(5-OP-RU)-MR1 suggested that only the uracil ring and the α-iminocarbonyl of 5-OP-RU (**9**) were essential for MR1 binding, whereas the ribityl chain was solvent-exposed (Fig. 1*B*). Similarly, 6-formylpterin (6-FP) and acetyl-6-formylpterin (Ac-6-FP) contain no ribityl chain yet also bind to MR1 (3, 21, 22). We had previously created a stable and functional analog of 5-OP-RU (JYM72, compound **10**) (Fig. 1*B*) by replacing its exocyclic nitrogens with carbons (5). Based on this stable compound, we designed MAgA-TAMRA (compound **8**) (Fig. 1*A*) with the uracil ring and the unsaturated carbonyl moiety of JYM72 to mimic key MR1-binding components of 5-OP-RU, and the TAMRA fluorophore substituting for the ribityl group. The fluorophore was appended to the uracil ring via a tether designed to be long enough to minimize interference from the fluorophore with binding of MAgA-TAMRA to MR1. The tether incorporated a triazole to facilitate fluorophore attachment, a glycine-based linker with two polar amides to improve water solubility, and a four-carbon spacer to separate the glycine unit from the MR1 binding motif.

MAgA-TAMRA (JYM20 in the chemical literature) was synthesized by first ring-opening glutaric anhydride with methanol (step *a* in Fig. 1*A*), then activation with oxalyl chloride (step *b* in Fig. 1*A*) to form the spacer (compound **1**). Uracil ring formation required a two-carbon extension of **1** with Meldrum's acid (step *c* in Fig. 1*A*), methanolysis to **2** (step *d* in Fig. 1*A*), cyclization with thiouracil (step *e* in Fig. 1*A*), and then hydrolysis/desulfurization to uracil **3** (step *f* in Fig. 1*A*). The glycine-alkyne linkers (**4**, two steps from Boc-Gly) were attached to give **5** (step *g* in Fig. 1*A*). Hydroxymethylation with formalin (step *h* in Fig. 1*A*), oxidation with cerium ammonium nitrate (step *i* in Fig. 1*A*), and then treatment with stabilized Wittig reagent **6** installed the Schiff base-forming group to give **7** with complete alkene stereospecificity (step *j* in Fig. 1*A*). Finally, the TAMRA fluorophore was attached via triazole formation to produce **8** (step *k* in Fig. 1*A*; see also *Materials and Methods*), which was very stable in aqueous solution over 24 h (PBS, 37 °C, pH 7.4) (*SI Appendix*, Fig. S1*D*).

To verify that MAgA-TAMRA behaved like 5-OP-RU, we compared their uptake by cells, capture by MR1, and presentation at the cell surface. MAgA-TAMRA accumulated in cells with similar kinetics to 5-OP-RU, but was gradually lost from cells after removing it from culture medium (Fig. 1*C*), and 37 °C was required for cell uptake (Fig. 1*D*). C1R and C1R.MR1 cells incubated with MAgA-TAMRA generated MR1–MAgA-TAMRA that was detected on the cell surface with antisera against TAMRA (αTAMRA). This was dependent on MR1 expression (Fig. 1*C*) and on trafficking from the ER, since brefeldin A (BFA) blocked detection (Fig. 1*E*). FRET, between MAgA-TAMRA and Alexa Fluor 647 conjugated to anti-MR1 but not to anti-MHC-II, indicated that surface MAgA-TAMRA was bound specifically to MR1 (Fig. 1*F*). MR1–MAgA-TAMRA did not activate the MAIT cell TCR (clone A-F7) (23) (Fig. 1*G*), consistent with the absence of TCR-binding ribityl chain. However, like Ac-6-FP (22), it could block activation by 5-OP-RU (Fig. 1*G*), consistent with competitive binding to MR1. These experiments confirm that MAgA-TAMRA is a bona fide MR1-binding ligand that can be captured and presented at the cell surface by MR1.

MR1–Ligand Complex Formation Occurs inside the ER. We sought to determine where MR1–ligand complex formation takes place in cells by combining microscopy and biochemical techniques.

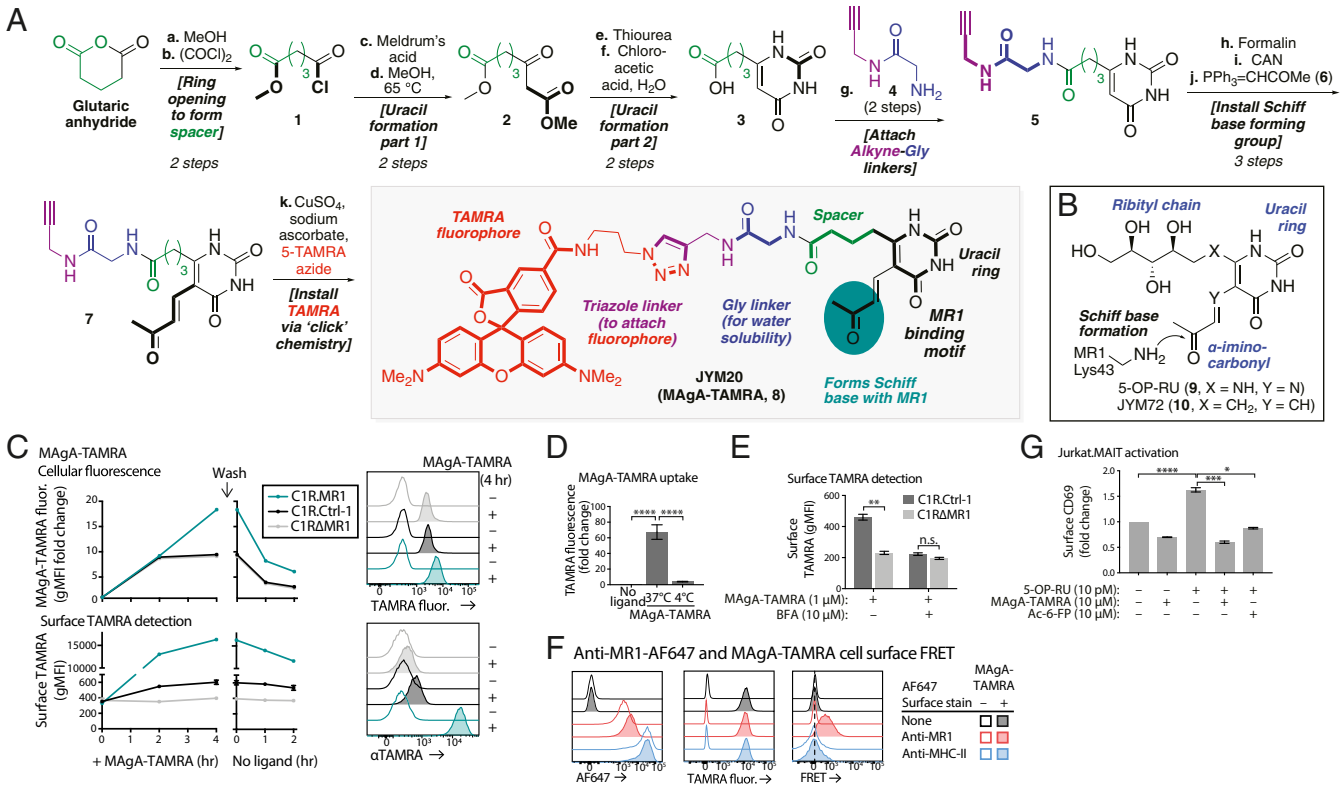

Fig. 1. Design and chemical synthesis of a fluorophore-labeled MR1 ligand. (*A*) Chemical synthesis of a labeled antigen analog (MAgA-TAMRA, **8**) from glutaric anhydride. A four-carbon spacer (green) extended the fluorophore and linker units away from a putative MR1 binding motif (black) based on JYM72 (**10**). A glycine-based linker (blue) was employed to improve ligand water solubility. TAMRA (red) was linked to the ligand via a triazole moiety (purple) using robust click chemistry. (*B*) 5-OP-RU (**9**) is a chemically unstable and weakly fluorescent MR1 ligand. JYM72 (**10**) is a water-stable analog that is highly fluorescent and functionally similar to 5-OP-RU. (*C*) C1R cells expressing Cas9 and a nontargeting single-guide RNA (sgRNA; C1R.Ctrl-1, black), a clonal knockout for MR1 (C1RΔMR1, gray), or cells overexpressing MR1 (C1R.MR1, green) were incubated with MAgA-TAMRA (1 μM) for 4 h, then washed and cultured for a further 2 h without ligand. Cellular fluorescence (*Upper*) was measured by flow cytometry by excitation with 561-nm laser and 582/15 emission filter, and surface TAMRA detected with anti-TAMRA antisera (*Lower*). Representative histograms are shown (*Right*). (*D*) C1R cells were incubated for 4 h in media alone (no ligand) or with 10 μM MAgA-TAMRA at 37 °C or 4 °C. Fluorescence was measured by flow cytometry. (*E*) C1R.Ctrl-1 or C1RΔMR1 cells were incubated with MAgA-TAMRA (1 μM) for 4 h in the presence or absence of BFA, followed by detection of surface TAMRA. (*F*) C1R.MR1 cells were incubated (shaded histograms) or not (empty histograms) with 10 μM MAgA-TAMRA for 4 h, then stained with Alexa Fluor 647 (AF647)-conjugated anti-MR1 (red) or anti MHC-II (blue) or unstained (black). Fluorescence was measured by flow cytometry for AF647, TAMRA, and FRET. (*G*) C1R.MR1 cells were coincubated with Jurkat cells transduced with a MAIT TCR (Jurkat.MAIT) and the indicated concentrations of MR1 ligands overnight, followed by measurement of CD69 surface expression on Jurkat.MAIT cells by flow cytometry. Data are mean ± SEM and representative of at least two independent experiments (*C*–*F*) or combined data for two experiments (*G*). Statistical significance calculated using one-way ANOVA and multiple comparison test where $*P < 0.05$, $**P < 0.01$, $***P < 0.001$, and $****P < 0.0001$, or not significant (n.s.).

MR1–GFP fusion molecules, expressed in HeLa and A549 airway epithelial cells, showed a diffuse ER-like distribution (Fig. 2*A* and *SI Appendix*, Fig. S2*A*), as found in C1R cells (14). A 10-min exposure of cells to MAgA-TAMRA, followed by fixation but without permeabilization, showed a punctate endosomal-like distribution that did not localize with MR1–GFP (Fig. 2*A* and *SI Appendix*, Fig. S2*A*). MAgA-TAMRA colocalized with the macropinocytosis marker, fluorescence-labeled dextran (*SI Appendix*, Fig. S2*B*), suggesting that its initial uptake into cells was nonspecific. When cells were permeabilized before microscopy, the vast majority of TAMRA signal was lost, suggesting permeabilization caused release of free MAgA-TAMRA from endosomes. Detection of MAgA-TAMRA in permeabilized cells required incubation for at least 2 h before analysis, but fluorescence was weak and it colocalized with MR1–GFP in an ER-like pattern (Fig. 2*B* and *SI Appendix*, Fig. S2*C*) but did not localize with the Golgi, early, or late endosomes (*SI Appendix*, Fig. S2*B*). These results indicate that MAgA-TAMRA is efficiently transported into cells via pinocytosis, and a small fraction reaches the ER although we could not establish how. Regardless of the mechanism involved, our main goal was to identify where the ligand binds to MR1.

Direct binding to MR1 was shown by incubating MAgA-TAMRA with C1R.MR1 cells and performing immunoprecipitation (IP) using αTAMRA (Fig. 2*C*). MR1 specifically interacted with MAgA-TAMRA, but not with TAMRA alone (Fig. 2*C*, lane 1). No complexes could be pulled-down with αTAMRA from cells expressing similar levels (14) of MR1 with a K43A or K43R mutation that prevents covalent bonding to MAgA-TAMRA (Fig. 2*C*).

In the absence of VitBAg, most MR1 glycoproteins remain inside the ER and are sensitive to endoglycosidase (endo) H, shown in SDS/PAGE by reduced size of MR1 due to enzymatic elimination of carbohydrate (*SI Appendix*, Fig. S3*A*) (14). Most MR1–MAgA-TAMRA immunoprecipitated with αTAMRA after 60 min culture with MR1-expressing cells were also endo H-sensitive, and became endo H-resistant after 2 h in the absence of the ligand (Fig. 2*D*). This indicates that MR1 primarily loads exogenous metabolites in the ER and then traffics through the Golgi. To support this conclusion, we used a proximity ligation assay (PLA), which produces fluorescence when two

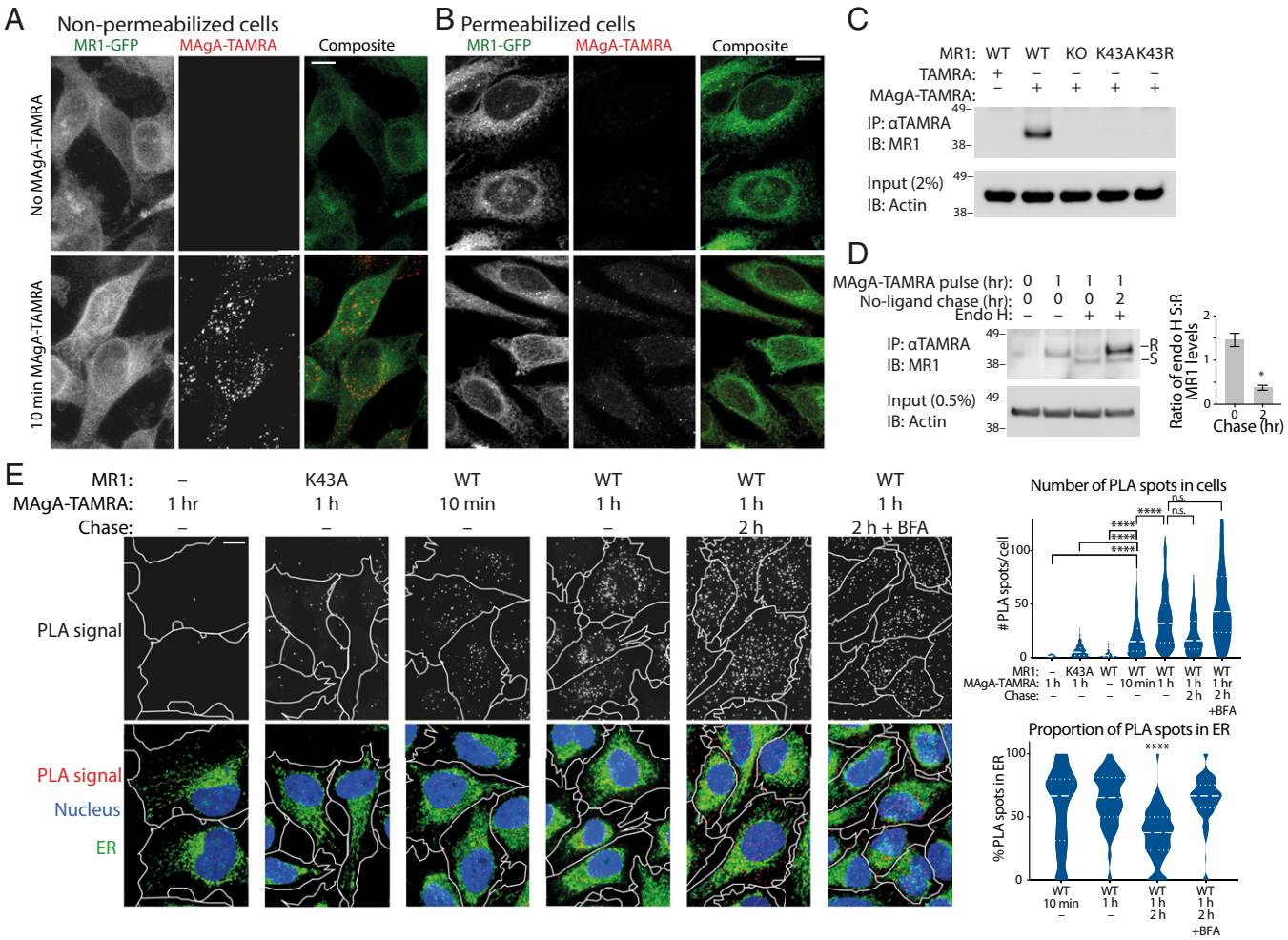

Fig. 2. MAgA-TAMRA reveals loading inside the ER. (*A*) HeLa cells transfected with MR1–GFP (HeLa.MR1–GFP; green) were cultured without ligand (*Upper*) or with 25 μM MAgA-TAMRA (red) for 10 min (*Lower*), then fixed and imaged without permeabilization. Shown are maximum projections from *z*-stacks. (*B*) HeLa.MR1–GFP cells (green) were cultured without ligand or with 25 μM MAgA-TAMRA (red) for 2 h, then fixed and permeabilized with 0.05% saponin prior to imaging. Shown are maximum projections from *z*-stacks. (*C*) C1R cells transfected with WT MR1 or Lys43 mutants (K43A or K43R) or MR1 KO cells were incubated with MAgA-TAMRA or TAMRA alone for 2 h. MAgA-TAMRA was immunoprecipitated with αTAMRA and then immunoblotted for MR1 (*Upper*). Input was immunoblotted for actin to control for loading (*Lower*). (*D*) C1R cells expressing endogenous levels of MR1 were incubated with or without MAgA-TAMRA for 1 h, then washed and further cultured without ligand for 2 h. MAgA-TAMRA was immunoprecipitated (IP) with αTAMRA, treated with or without endo H, and then immunoblotted (IB) for MR1 with mAb 8G3. A fraction of the pre-IP lysate (0.5%) was immunoblotted for actin as a loading control. The levels of endo H-sensitive (S) to -resistant (R) MR1 levels were quantified and the ratio of these from four experiments are represented (*Right*). Statistical significance calculated using a paired *t* test, where $*P = 0.013$. (*E*) HeLa cells transfected without, or with WT MR1 or K43A mutant were incubated with or without 50 μM MAgA-TAMRA for the indicated times, then fixed or washed and cultured for a further 2 h without ligand (±BFA). After permeabilization, cells were stained with ER-green probe, mouse anti-MR1 (mAb 8F2.F9), and rabbit αTAMRA then subjected to a PLA. Each PLA spot represents a molecular interaction between MR1 and MAgA-TAMRA, and these were enumerated (violin plots). For each cell, the total number of spots was counted including the proportion inside the ER. (Scale bar: *A, B,* and *E,* 10 μm.) Statistical significance calculated using a one-way ANOVA and multiple comparison test, where $****P < 0.0001$ or not significant (n.s.). Data are shown as mean ± SEM (*D* and *E*) and are representative of two independent experiments (*A*–*C*) or the combined data of four (*D*) or two (*E*) independent experiments.

molecules are within 40 nm (24). Incubating cells with MAgA-TAMRA for 10 min resulted in MR1–MAgA-TAMRA complexes, detectable by PLA as distinct puncta that increased in number over 1 h (Fig. 2*E*). There was negligible signal in cells not overexpressing MR1 or those expressing mutant MR1-K43A (*SI Appendix*, Fig. S2*D*) after 1-h coincubation (Fig. 2*E*), consistent with the requirement for the K43 ε-amino group in MR1 for covalent bonding to MAgA-TAMRA. The PLA puncta observed in WT cells incubated for 10 min or 1 h with MAgA-TAMRA colocalized with the ER, but after removal of the ligand and further incubation for 2 h, the number of complexes at this location was halved. This is consistent with exit of the MR1–MAgA-TAMRA complex from the ER and entry into the secretory pathway, aligning with the observation that MR1 molecules acquire endo H resistance as they cross the Golgi (Fig. 2*D*). To confirm this, we performed the 2 h chase in the presence of BFA to block transit through the Golgi, which caused retention of the MR1–MAgA-TAMRA PLA signal within the ER (Fig. 2*E*). These results establish binding of MR1 to extracellular ligands within the ER followed by egress to the cell surface, and highlight the application of a novel fluorophore-labeled, epitope-tagged MR1 ligand to identify the subcellular location of MR1-Ag loading.

A Monoclonal Antibody Reveals Distinct MR1 Conformers inside the ER. By analogy with MHC-I, the heavy chain (HC) of MR1 molecules is thought to undergo conformational change in the ER as it transitions from the free HC, to the HC–β_2m heterodimer, to

the fully-folded HC–β_2m–Ag trimeric complex (Fig. 3*A*). Suitable reagents have not previously been available to study this process. We have described a rabbit serum against the MR1 cytosolic tail (αMR1-CT) that recognizes all conformers, while the monoclonal antibody (mAb) 8F2.F9 is thought to recognize the fully-folded MR1 conformer ($MR1^{FOLDED}$) (Fig. 3*A*) (14, 25, 26). Sequential IP shows that not all MR1 is recognized by 8F2.F9. When this mAb was used to IP MR1 from cells not incubated with VitBAg, we obtained MR1 molecules that were endo H-sensitive and bound to β_2m (Fig. 3*C*, lanes 1 and 2). However, this mAb left behind a larger fraction of MR1 that could be recovered with αMR1-CT, but did not coprecipitate with β_2m (Fig. 3*C*, lane 5), and might correspond to a β_2m-free conformer that lacked the 8F2.F9 epitope ($MR1^{OPEN}$) (Fig. 3*A*). As a control, lysates that were first IP with αMR1-CT did not leave behind recoverable MR1 (Fig. 3*C*, lanes 4 and 5).

We sought to produce a new mAb specifically raised against the "empty" $MR1^{OPEN}$ conformer, analogous to mAb HC10 generated against empty MHC-I (27–29), or to anti-mouse MR1 mAb, 4E3 (26). We immunized $MR1^{-/-}$ mice with a peptide corresponding to MR1 α1-domain residues P48-R61 (analogous to the HC10 epitope in MHC-I) (Fig. 3*B*), and generated mAb 8G3. This mAb captured only β_2m-free MR1 molecules, both during a primary IP (Fig. 3*C*, lanes 1 and 2) and during a secondary IP following IP with 8F2.F9 (Fig. 3*C*, lane 3). Conversely, after a primary IP with 8G3, MR1–β_2m complexes remained in the lysates and these could be sequentially immunoprecipitated with either 8F2.F9 or αMR1-CT (Fig. 3*C*, lanes 4 and 5, respectively).

These experiments show that, in the absence of VitBAg, two distinct MR1 conformers occur in the ER: one unbound to β_2m and recognized by 8G3 ($MR1^{OPEN}$) and one bound to β_2m and recognized by 8F2.F9 ($MR1^{FOLDED}$) (Fig. 3*A*). Addition of Ac-6-FP, causing the formation of trimeric MR1–β_2m–ligand complexes (14), leads to the expected loss of $MR1^{OPEN}$ recognized by 8G3 and an increase in 8F2.F9-reactive $MR1^{FOLDED}$, a large fraction of which became endo H-resistant (Fig. 3*C*, lanes 6–9). By immunoblotting, the mAb 8G3 detected the HC of both mouse (*SI Appendix*, Fig. S3*B*) and human (Fig. 2*D*) MR1–ligand complexes denatured in SDS/PAGE, further supporting the notion that the epitope recognized by 8G3 is a conserved linear amino acid sequence exposed to the solvent in the $MR1^{OPEN}$ conformer that becomes hidden by a conformational change in $MR1^{FOLDED}$.

MR1 Binds to Components of the Peptide Loading Complex. Next, we hypothesized that the two MR1 conformers contained inside the ER were stabilized by chaperones to maintain a pool of ligand-receptive MR1. Loss of these chaperones might reduce this pool and impair efficient presentation of VitBAg. To investigate this, two unbiased approaches were taken. First, we sought steady-state binding partners of MR1 using anti-GFP antibodies to IP MR1–GFP molecules from transfected C1R cells (C1R.MR1–GFP) and applied a label-free quantitative (LFQ) mass spectrometry (MS) approach to identify coprecipitating proteins. As a negative control to rule out nonspecific or GFP-specific protein interactions, we obtained in parallel GFP IPs from C1R.MR1 cells transfected with nonfused MR1 and GFP (Fig. 4*A*). Several proteins were identified as significantly enriched in MR1–GFP precipitates (*SI Appendix*, Table S1) in addition to MR1 and β_2m. These included all members of the MHC-I peptide loading complex (PLC): tapasin (TPN), the disulfide isomerase ERp57 (also known as PDIA3), transporter associated with antigen processing (TAP) subunits 1 and 2, and calreticulin (CRT) (17), as well as HLA-C (the sole MHC-I HC expressed by C1R cells). Other binding partners included calnexin (CANX) and UDP-glucose:glycoprotein glucosyltransferase 1 (UGGT1), which perform glycoprotein quality control for MHC molecules (30) and several ER-resident chaperones, including other PDI isoforms PDIA1, -4, and -6, (*SI Appendix*, Table S1).

Immunoblot analysis of proteins coprecipitating with MR1–GFP and MR1 (not fused to GFP) confirmed the presence of PLC components and also MHC-I (HLA-C) HC (Fig. 4 *B* and *C*). Since the PLC accommodates two MHC-I molecules (31), this suggests that MR1 can replace one or possibly both HLA HC in the PLC. The association between MR1 and the PLC decreased after exposure of cells to Ac-6-FP (Fig. 4*B*), indicating ligand binding and that adoption of the completely folded conformation leads to release of MR1 from the PLC for ER egress. We confirmed the interaction of MR1 with the PLC and HLA-B or HLA-C in THP1 cells which, unlike C1R, have intact HLA expression (32) (Fig. 4*D*). Reciprocal IP of TPN, and TAP1 from C1R and THP1 cells also retrieved MR1 (Fig. 4*E*).

TPN-related protein (TAPBPR) is an MHC-I chaperone structurally similar to the PLC component TPN, but is not part of the PLC. We investigated whether TAPBPR also coprecipitated with MR1 and, while it was not identified by MS, whether we could detect it by immunoblotting (Fig. 4*B*). We could coprecipitate TAPBPR with MR1 and, intriguingly, this interaction did not diminish after incubation with Ac-6-FP (Fig. 4*B*), consistent with the notion that TAPBPR may chaperone MR1 outside the ER as it does MHC-I (33). However, an interaction between MR1 and TAPBPR could not be demonstrated by IP of MR1 from THP1.MR1 cells (Fig. 4*D*), nor by IP of TAPBPR from either C1R

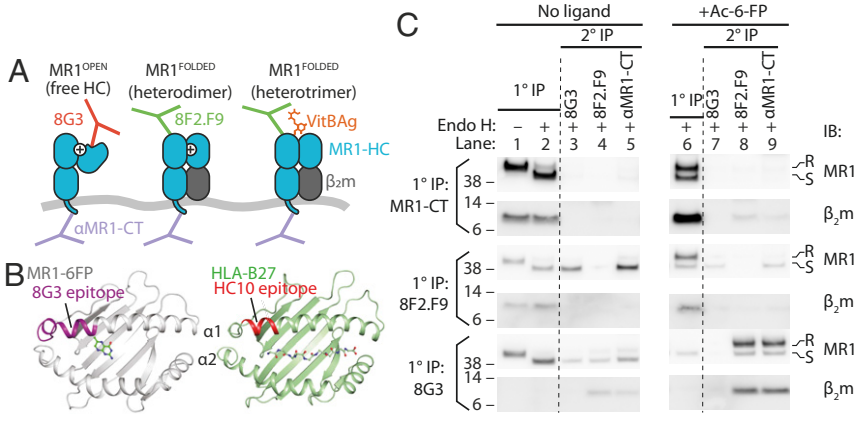

Fig. 3. A novel antibody against MR1 reveals a β_2m-deficient HC conformer exists in the ER. (*A*) Schematic representation of the conformational states of steady-state MR1 as distinguished by each antibody. MR1-HC (blue) shown bound or not to β_2m (gray), and empty or loaded with VitBAg. The charged lysine-43 side chain in empty MR1-HC is indicated by a plus symbol (+). (*B*) Structural alignment of MR1–β_2m-6-FP (PDB ID code 4GUP; gray) and HLA-B27 (PDB ID code 1HSA; green) with their bound antigens. Epitopes for mAbs 8G3 and HC10 are highlighted in purple and red, respectively. (*C*) C1R cells transfected with MR1 were treated without ligand (lanes 1–5) or with Ac-6-FP (lanes 6–9) for 6 h, then lysed and sequential IPs performed using antibodies against the cytosolic tail (αMR1-CT) or conformational-specific mAbs 8G3 or 8F2.F9. After the primary IP (1°) was carried out (lanes 1, 2, 6) the remainder was then subjected to a secondary IP (2°) with each antibody (lanes 3–5, 7–9). Precipitates were treated with endo H or not, then separated by SDS/PAGE and immunoblotted with αMR1-CT or anti-β_2m. Endo H-resistant (R) or -sensitive (S) MR1 are indicated.

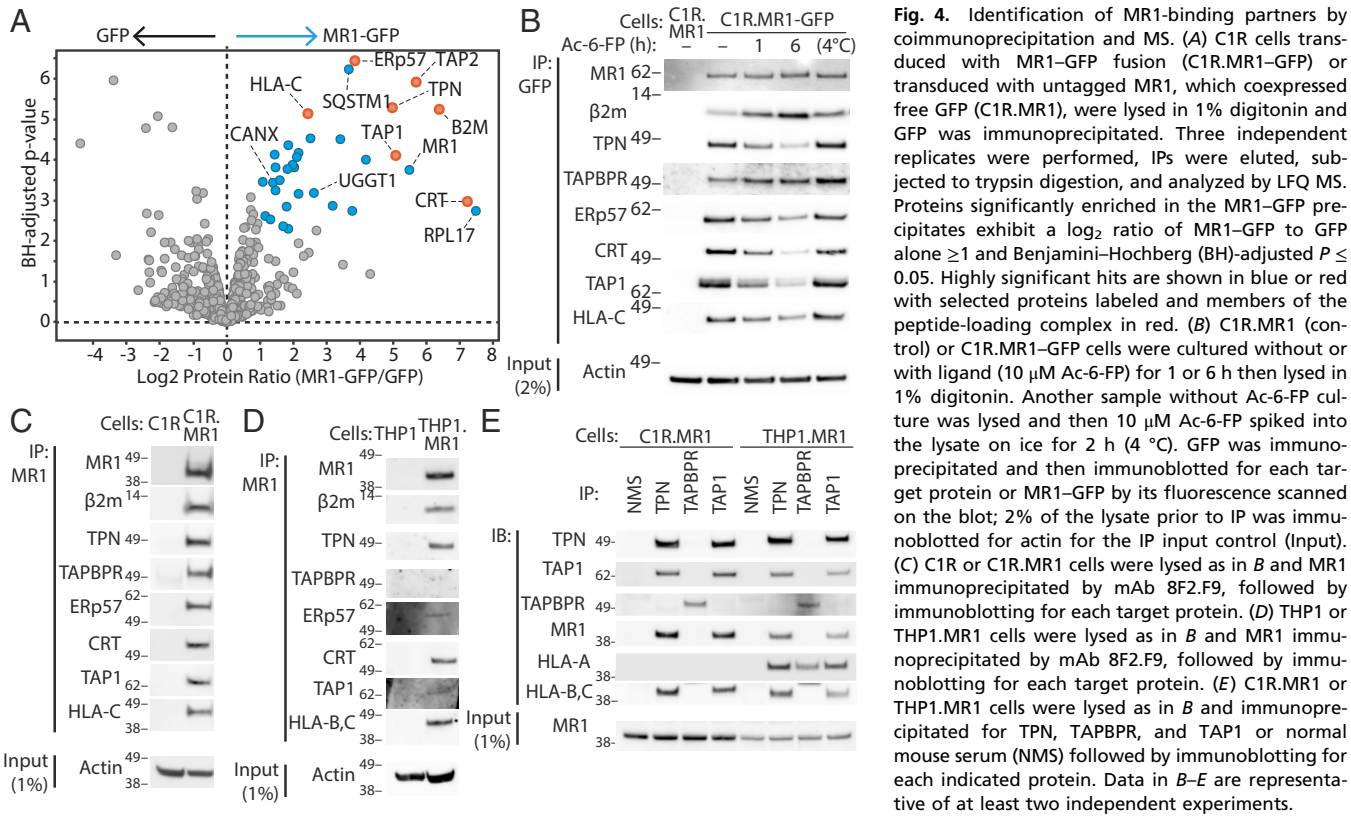

Fig. 4. Identification of MR1-binding partners by coimmunoprecipitation and MS. (*A*) C1R cells transduced with MR1–GFP fusion (C1R.MR1–GFP) or transduced with untagged MR1, which coexpressed free GFP (C1R.MR1), were lysed in 1% digitonin and GFP was immunoprecipitated. Three independent replicates were performed, IPs were eluted, subjected to trypsin digestion, and analyzed by LFQ MS. Proteins significantly enriched in the MR1–GFP precipitates exhibit a $\log_2$ ratio of MR1–GFP to GFP alone ≥1 and Benjamini–Hochberg (BH)-adjusted $P \leq 0.05$. Highly significant hits are shown in blue or red with selected proteins labeled and members of the peptide-loading complex in red. (*B*) C1R.MR1 (control) or C1R.MR1–GFP cells were cultured without or with ligand (10 μM Ac-6-FP) for 1 or 6 h then lysed in 1% digitonin. Another sample without Ac-6-FP culture was lysed and then 10 μM Ac-6-FP spiked into the lysate on ice for 2 h (4 °C). GFP was immunoprecipitated and then immunoblotted for each target protein or MR1–GFP by its fluorescence scanned on the blot; 2% of the lysate prior to IP was immunoblotted for actin for the IP input control (Input). (*C*) C1R or C1R.MR1 cells were lysed as in *B* and MR1 immunoprecipitated by mAb 8F2.F9, followed by immunoblotting for each target protein. (*D*) THP1 or THP1.MR1 cells were lysed as in *B* and MR1 immunoprecipitated by mAb 8F2.F9, followed by immunoblotting for each target protein. (*E*) C1R.MR1 or THP1.MR1 cells were lysed as in *B* and immunoprecipitated for TPN, TAPBPR, and TAP1 or normal mouse serum (NMS) followed by immunoblotting for each indicated protein. Data in *B*–*E* are representative of at least two independent experiments.

or THP-1 cells overexpressing MR1. Since TAPBPR has little or no demonstrable binding to some HLA-B molecules but still has peptide-editing ability for these proteins (34), we considered that TAPBPR may still chaperone MR1 but with weak affinity.

The second unbiased approach we used to identify accessory proteins for MR1 presentation was a genome-wide CRISPR/Cas9 loss-of-function library screen. We sought to identify gene deletions that decreased MR1 presentation of 5-OP-RU. Here, C1R (WT) cells were transduced with the GeCKO v1 library (35) in triplicate, showing virtually all component single-guide RNAs (sgRNAs) were represented (*SI Appendix*, Fig. S4). The library cells were cultured with 5-OP-RU and the 5% of cells with the lowest expression of MR1 ($MR1^{LOW}$) were sorted, expanded in culture, and then selected again for a second time. These two rounds of selection resulted in an enrichment of a distinct population of cells with low MR1 expression (Fig. 5*B*). The sgRNAs contained in the selected cells were amplified and identified by sequencing (Fig. 5*C*). These included two sgRNAs targeting *mr1*, one for *b2m*, four for *tapbp* (encoding TPN), and two for *crt* and *tap1* (Fig. 5*C* and *SI Appendix*, Table S2). Therefore, two unbiased approaches indicated that the components of the PLC participate in MR1 antigen presentation.

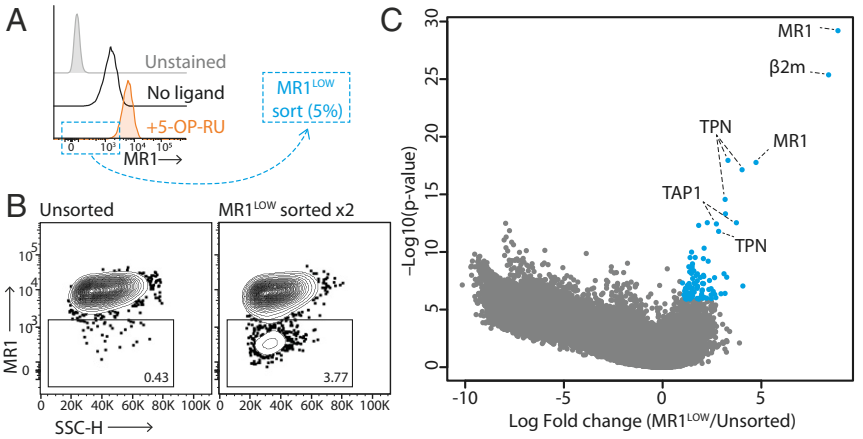

Fig. 5. Identification of proteins required for MR1 surface expression by genome-wide CRISPR/Cas9 loss-of-function screen. (*A*) C1R cells were transduced with lentivirus containing a GeCKO V1 human CRISPR KO library in triplicate. Cells were then cultured with 0.5 μM 5-OP-RU (orange histogram) for 4 h and stained for surface MR1. MR1-low cells (5% of total population) were sorted and expanded then sorted again for a second time. MR1 levels in cells cultured without ligand (black) compared to after 5-OP-RU culture (orange) and unstained cells (gray) are shown. Shown is a representative of three replicates. (*B*) After two rounds of sorting for MR1-low cells, the unsorted (*Left*) and twice-sorted (*Right*) pools were cultured with 0.5 μM 5-OP-RU for 4 h and stained for surface MR1, showing an enrichment for cells which express low surface MR1 levels. Shown is a representative of three replicates. (*C*) The viral integration site encompassing the sgRNA cassette was amplified and sequenced from each sample, and the twice-sorted compared to the unsorted pool samples. Shown is the plot of significance [$-\log_{10}(P$ value)] and fold-change ($\log_2$ fold-change; >0 denotes enrichment in the sorted samples) for each sgRNA. The most significant and enriched hits above cutoff values are highlighted in blue.

TPN and TAPBPR Cooperate to Enhance MR1 Surface Expression. Next, we sought to confirm the role of PLC components in MR1 expression and antigen presentation by generating clonal CRISPR/Cas9-modified C1R cell lines with defined loss-of-expression mutations. TAP plays a dual role in the PLC: as a transporter of MHC-I ligands from the cytosol into the ER and as a scaffold for the assembly of the other components of the PLC (31). Therefore, it was unsurprising that deleting TAP (Fig. 6*A*) had a profound effect on MHC-I expression (Fig. 6*B*) without affecting the expression of other surface proteins, MHC-II or transferrin receptor (TfR) (Fig. 6*B*). The deletion of TAP did not decrease MR1 surface expression either in the absence or presence of 5-OP-RU, and it did not affect MAgA-TAMRA presentation (Fig. 6*B*), indicating that TAP is not essential for ligand access into the ER. In contrast, deletion of TPN (Fig. 6*A*) had a profound effect not only on MHC-I expression as expected (36) (Fig. 6*B*), but also on MR1 expression, especially in the presence of 5-OP-RU with a significant loss of more than 30% (Fig. 6*B*). This effect was confirmed by CRISPR/Cas9 deletion from primary normal human bronchial epithelial (NHBE) cells obtained from two different human donors. In the absence of MR1 ligand, those NHBE cells that expressed low levels of MHC-I (a surrogate marker of TPN elimination) also had reduced MR1 compared to their MHC-I^{high} (nonmutant) counterparts with and without 5-OP-RU, while TfR was unaffected (Fig. 6*C*). The irradiation-induced TPN-deficient cell line, 721.220 (37, 38) had low expression of MR1 and MHC-I, and these were significantly increased by TPN expression (721.220.TPN) (39) (Fig. 6*D*).

This demonstrates a role for TPN in MR1 expression. Considering the PLC component CRT cooperates with TPN to ensure efficient loading of MHC-I with high-affinity cargo (40, 41), and that we detected CRT binding to MR1 (Fig. 4), we tested if deletion of CRT similarly affected MR1 expression (*SI Appendix*, Fig. S5). We did not find an effect of CRT deletion on the level of MR1 either in the absence or presence of 5-OP-RU, suggesting that the role of TPN in MR1 expression is independent of CRT. Our IP analysis indicated TAPBPR may also transiently interact with MR1 (Fig. 4*B*). CRISPR/Cas9 mutant C1R clones lacking TAPBPR expression displayed normal MR1 levels and also expressed normal levels of MHC-I (Fig. 6*B*). Therefore, TAPBPR does not appear to play a critical role in overall surface expression of either of these two molecules. However, it was previously shown that in the absence of TPN, more MHC-I associates with TAPBPR (42), hence we reasoned that TPN or TAPBPR might compensate for the loss of the other. Indeed, MR1 expression was significantly reduced (~50%) in TPN-TAPBPR double-deficient cells both in the absence or the presence of MR1 ligand, as was the surface presentation of MR1

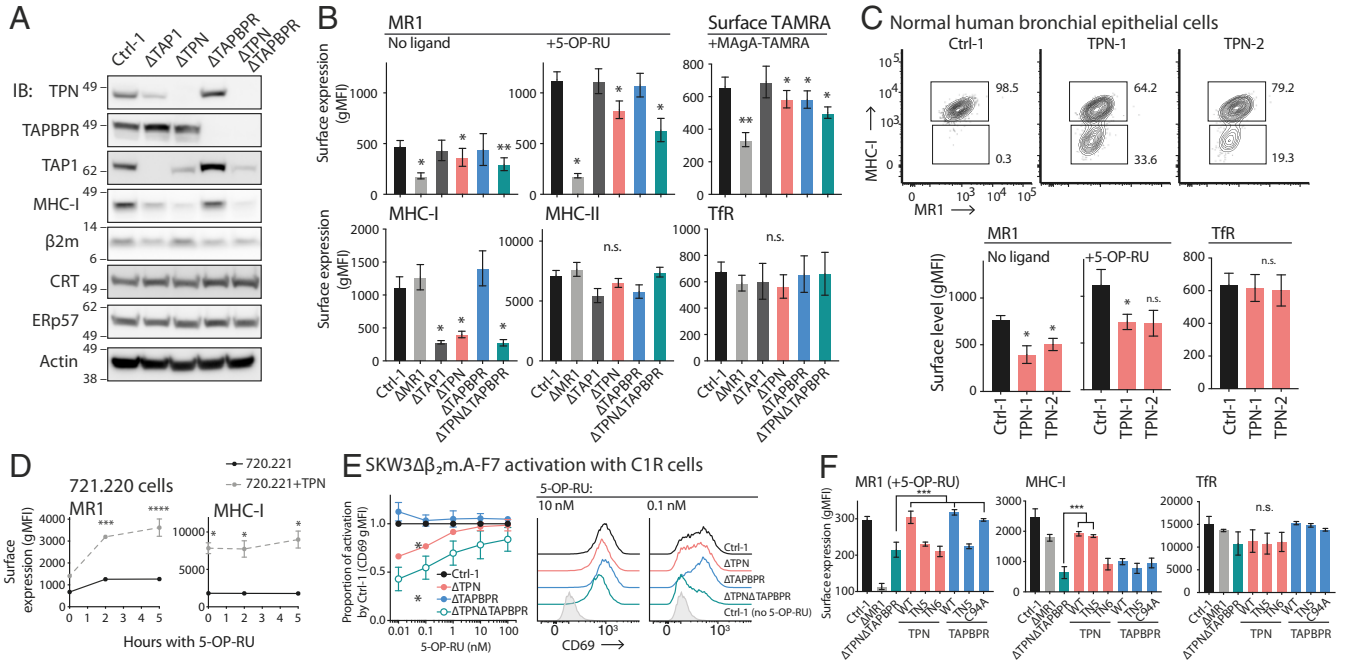

Fig. 6. The chaperones TPN and TAPBPR support MR1 expression. (*A*) Single-cell clones of C1Rs knocked out (Δ) for TAP1, TPN, TAPBPR, or both TPN and TAPBPR were compared to cells transduced with a control nontargeting sgRNA (Ctrl-1). Cells were lysed and immunoblotted (IB) for detection of the indicated proteins. (*B*) Cells from *A* were cultured with or without 5-OP-RU or MAgA-TAMRA for 4 h, and levels of MR1 or surface TAMRA, or MHC-I, MHC-II, and TfR were measured by flow cytometry. (*C*) NHBE cells were transfected with Cas9–RNA ribonucleoprotein complexes targeting either TPN (TPN-1, -2) or a control nontargeting RNA sequence (Ctrl-1). The expression of MHC-I, MR1, or TfR was measured by flow cytometry after culture with or without 5-OP-RU. The TPN KO cells were identified by low MHC-I levels, and the MR1 surface expression of these cells is represented in the bar graphs (*Right*) compared to MHC-I–normal Ctrl-1–transfected cells. (*D*) TPN-deficient 721.220 cells or the same cells transfected with TPN (721.220.TPN) were cultured with 5-OP-RU for the indicated times and the levels of MR1 and MHC-I were measured by flow cytometry. (*E*) C1R.Ctrl-1 or KO cell lines were incubated with the MAIT cell surrogate (SKW3 cells deficient in β2m, transduced with the MAIT cell T cell receptor A-F7; SKW3Δβ$_2$m.A-F7). 5-OP-RU was added at the indicated amounts for 16 h and the amount of CD69$^+$ SKW3 cells were measured by flow cytometry. The proportion of activation with each cell line is shown relative to C1R.Ctrl-1 for each concentration and representative histograms of CD69 levels are shown (*Right*). (*F*) C1RΔTPNΔTAPBPR cells were transduced with WT or mutant forms of TPN (TN5, TN6) or TAPBPR (TN5, C94A). Cells were cultured with or without 5-OP-RU and levels of MHC-I, MR1 and TfR were measured by flow cytometry. Significant differences to ΔTPNΔTAPBPR indicated by the asterisks. Data are shown as mean ± SEM and are representative of at least two independent experiments (*B* and *D*–*F*) or the mean ± SEM of two donors in two independent experiments (*C*). Statistical significance calculated using one-way (*B*, *C*, and *F*) or two-way (*D* and *E*) ANOVA and multiple comparison test where significance denoted by $*P < 0.05$, $**P < 0.01$, $***P < 0.001$, and $****P < 0.0001$, or not significant (n.s.).

loaded with MAgA-TAMRA (Fig. 6*B*), while expression of MHC-II and TfR was unaffected.

We then investigated if the effect of TPN and TAPBPR on MR1 surface expression also translated to VitBAg presentation to a MAIT cell surrogate. For this, we expressed the MAIT cell receptor clone A-F7 (23) in SKW3 cells, and deleted β_2m to prevent these cells from also presenting MR1 and autoactivating (SKW3Δβ_2m.A-F7 cells). We incubated these cells with C1R cells lacking expression of TPN, TAPBPR, or both, with different amounts of 5-OP-RU. Assessment of CD69 up-regulation in SKW3Δβ_2m.AF7 cells as a surrogate of MR1–5-OP-RU complex recognition revealed that at low levels of 5-OP-RU, TPN-deficient cells showed a significantly reduced presentation. This was further reduced when both TPN and TAPBPR were deleted, while no effect was caused by the absence of TAPBPR alone (Fig. 6*E*).

We could rescue MR1 expression in cells lacking endogenous TPN and TAPBPR by transfecting WT TPN or TAPBPR genes, restoring MR1 to WT levels (Fig. 6*F*). We reasoned that if TPN and TAPBPR interact directly with MR1 as they do with MHC-I (42, 43), the mutations known to affect their interaction with MHC-I would also affect their interaction with MR1. Indeed, mutant versions of TPN or TAPBPR known to bind little or not at all to MHC-I [TPN-TN5, -TN6 (43), and TAPBPR-TN5 (42)] did not increase MR1 expression (Fig. 6*F*). Furthermore, the TAPBPR-C94A mutant, which can associate with MHC-I but not with UGGT1 (44), could still rescue MR1 expression equivalently to TAPBPR-WT, suggesting that an UGGT1–TAPBPR interaction is not required for the rescue of MR1 expression. Expression of the TPN or TAPBPR forms did not affect TfR, and only TPN-WT and the TN5 mutant could restore MHC-I expression (Fig. 6*F*). These data indicate that both TPN and TAPBPR influence MR1 expression via direct association mediated by similar structural regions to those involved in MHC I binding. They also show that, in the absence of TPN, TAPBPR can restore MR1 but not MHC-I expression.

In Silico Modeling of MR1 with TPN and TAPBPR. Next we used comparative homology modeling to predict how MR1 interacts with TPN and TAPBPR, based on the published crystal structures of MR1–β_2m-6-FP (3), TPN–MHC-I (31), and TAPBPR–MHC-I (45) (*SI Appendix*, Fig. S6). Because of the template-target high-sequence similarities, the generated models did not show major steric clashing. The best modeled structures of TPN–MR1 and TAPBPR–MR1 were selected based on the overall global and per residue quality and Ramachandran plots (*SI Appendix*). We found that MR1 adopted a similar orientation when interacting with each chaperone, and the MR1 regions that interacted with both chaperones were analogous to those involved in MHC-I (31, 45). These regions were located in the α2 and α3 domains of the MR1-HC (Fig. 7*A* and *SI Appendix*, Figs. S7 and S8), with similarities in the interacting residues shown to be important for chaperone–MHC-I interaction. Alignment of the MR1 amino acid sequence with TPN or TAPBPR-binding MHC-I allomorphs shows conservation in key residues in these interacting regions (*SI Appendix*, Figs. S7 and S8). In general, the interaction interface of MR1 with TAPBPR is quite broad and extensive compared to the interface with TPN, similar to that observed for their interactions with MHC-I.

The TPN–MR1 model predicts a network of strong electrostatic interactions between MR1 N123 and Q223 residues, analogous to the conserved N119 and Q226 of MHC-I, with the critical TPN R87 and C-terminal domain of TPN, respectively, thought to be important for TPN interaction (31) (*SI Appendix*, Fig. S7 *C* and *D*). For TAPBPR, two regions forming functionally important associations with MHC-I are the "jack hairpin" and "scoop loop," both of which interacted with MR1 in the model (*SI Appendix*, Figs. S6*A* and S8), with two key interacting residues in the former being conserved in MR1 and MHC-I (Q111 and D118) (*SI Appendix*, Fig. S8 *C* and *H*). While both TPN and TAPBPR C-terminal regions interacted with the MR1 α3 domain, the C-terminal domain of TAPBPR was rotated permitting an interaction directly with β_2m, compared to TPN, and this was similarly modeled previously for MHC-I (45). Of note, TPN did not interact with β_2m at all in our model (*SI Appendix*, Fig. S6*E*).

In comparison to the loaded MR1–β_2m-6-FP structure, the interaction with both chaperones opened the Ag-binding cleft, most notably at the α2-1 region (*SI Appendix*, Fig. S6*D*). This allowed the scoop loop of TAPBPR to interrogate the F′ pocket of the Ag-binding cleft, as shown for MHC-I (45). Interestingly no structural movements were predicted in the A′ pocket with either chaperone, where the known metabolites bind. The TPN-TN5 and -TN6 and the TAPBPR-TN5 mutations were found to be within the regions of contact with the α2 domain of MR1-HC (*SI Appendix*, Fig. S6 *E* and *F*), illustrating how these mutations may disrupt chaperone binding to MR1.

Chaperoning Activity of TPN and TAPBPR on ER-Resident MR1. Finally, we investigated the mechanism by which TPN and TAPBPR support MR1 surface expression. Our model for MR1 presentation of extracellular ligands predicts the most important factor to be the number of MR1 molecules within the ER that are available for ligand binding. To determine if the loss of the chaperones reduced this pool, we assessed the total amount of MR1 that could be immunoprecipitated from C1R cells lacking TPN, TAPBPR, or both, compared to WT cells. Transcription of the *mr1* gene in the three chaperone KO cell lines was comparable (*SI Appendix*, Fig. S9*A*), but we observed significant reductions in the amount of MR1 protein in all three lines, reaching 85% in the cells lacking both TPN and TAPBPR (Fig. 7*A*). Conversely, overexpression of TPN in 721.220 cells resulted in approximately a fivefold increase in the amount of MR1 protein (Fig. 7*B*), with no change in *mr1* transcription (*SI Appendix*, Fig. S9*B*). Thus, the role of TPN and TAPBPR in MR1 stabilization appeared more prominent than was inferred from the effect of their deletion on MR1 surface expression (Fig. 6).

Radiolabeling (pulse)-chase experiments were then performed to better characterize the effect of the deletions on the half-life of empty MR1 (Fig. 7*C*). Loss of TPN and TAPBPR had an additive effect on the survival of ER resident (endo H-sensitive) MR1 molecules generated during the pulse, and chased in the absence of ligands. This explains the reductions in total MR1 observed in the mutant cells (Fig. 7*A*). Addition of MR1 ligand Ac-6-FP during the chase induced similar formation of radiolabeled endo H-resistant molecules in WT and in chaperone-deficient cells, and the half-life of the resulting complexes was unaffected by the deletions (Fig. 7*C*). Thus, TPN and TAPBPR stabilize the pool of ER-resident MR1 molecules available for VitBAg capture, but do not affect the formation or survival of MR1–ligand complexes. The impairment in MR1 presentation in chaperone-deficient cells (Fig. 6) is therefore due to the reduction in the pool of ER-resident MR1 molecules available for recruitment to the cell surface in mutant cells, rather than to an impaired capacity of the existing molecules to bind ligand or to reduced stability of the resulting MR1–ligand complexes.

As shown above, we have found that ligand-free MR1 molecules are present within the ER in two distinct conformers, one bound ($MR1^{FOLDED}$) and the other unbound to β_2m ($MR1^{OPEN}$), which can be recognized by 8F2.F9 and 8G3 mAbs, respectively. We wondered whether TPN and TAPBPR could stabilize either of these two conformers or both. We carried out pulse-chase experiments with C1R.MR1 cells expressing or lacking both TPN and TAPBPR, and then immunoprecipitated sequentially the $MR1^{OPEN}$ followed by the $MR1^{FOLDED}$ conformer. The amount of

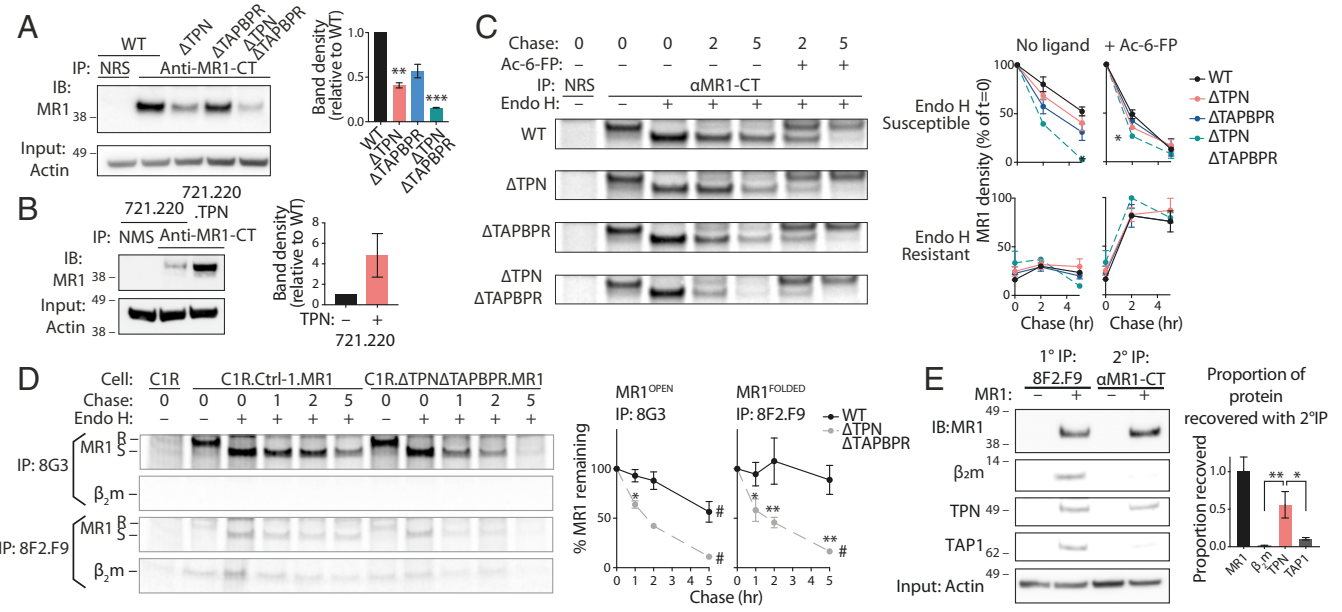

Fig. 7. TPN and TAPBPR stabilize an ER-resident conformational form of MR1. (*A*) MR1 was immunoprecipitated from C1R cell lines using αMR1-CT (or control with normal rabbit sera, NRS) and immunoblotted for MR1. The amount of MR1 was quantitated by densitometry. (*B*) The amount of total MR1 in 721.220 and the same cells overexpressing tapasin (721.220.TPN) was quantified as for *A*. (*C*) Autoradiogram of untreated or endo H-treated MR1 immunoprecipitated from WT (C1R.Ctrl-1) or KO lines overexpressing MR1 that had been metabolically radiolabeled with [^{35}S]methionine/cysteine and then chased for the indicated time with or without 5-OP-RU. (*D*) Ctrl-1 or ΔTPNΔTAPBPR KO cells overexpressing MR1 were metabolically radiolabeled with [^{35}S]methionine/cysteine and then chased for the indicated times then subjected to sequential IPs first with clone 8G3, then clone 8F2.F9. (*E*) C1R and C1R.MR1 were lysed in 1% digitonin and sequential IPs performed. After a primary IP (1° IP) was carried out with clone 8F2.F9 (lanes 1 and 2), the supernatant was then subjected to a secondary IP (2° IP) with antibodies against the cytosolic tail (αMR1-CT). Precipitates were separated by SDS/PAGE and immunoblotted with antibodies against MR1, TPN, TAP1, or β_2m. Data are the mean ± SEM of two (*B*) or three (A and *C*–*E*) independent experiments. Statistical significance calculated using one-way (*A* and *E*) or two-way (*C* and *D*) ANOVA and multiple comparison test. Significant differences from WT (*A*, *C*, and *D*) or MR1 (*E*) shown by $^{*}P < 0.05$, $^{**}P < 0.01$, or $^{***}P < 0.001$, or not significant (n.s.). Significant differences from 0 h shown by $^{\#}P < 0.05$.

MR1 that could be immunoprecipitated in the MR1$^{\text{FOLDED}}$ conformation from the two cell lines after the 30-min pulse was small (~10%) (Fig. 7*D* and *SI Appendix*, Fig. S9*C*). In WT cells, this fraction was long-lived, while in cells lacking TPN and TAPBPR, its half-life was <2 h (Fig. 7*D*). The MR1$^{\text{OPEN}}$ conformer had a shorter half-life than the MR1$^{\text{FOLDED}}$ one in WT cells (~5 h), but this also decreased to <2 h in the double-mutant cells (Fig. 7*D*). Therefore, TPN and TAPBPR can stabilize both MR1 conformers, although their effect on the folded conformer is more pronounced. We reasoned that if this were true, both forms would associate with the chaperones and potentially with the PLC. The mAb 8F2.F9 could IP MR1$^{\text{FOLDED}}$ from cell lysates prepared with the weak detergent digitonin or with the stronger detergent IGEPAL CA-630 (also known as Nonidet P-40) (*SI Appendix*, Fig. S9*D*). However, MR1 only coprecipitated with PLC components TPN and TAP when retrieved from digitonin lysates (Figs. 4 and 7*E*) likely because IGEPAL disrupts these molecular interactions. In contrast, mAb 8G3 could precipitate MR1 from IGEPAL cell lysates, but not from digitonin ones (*SI Appendix*, Fig. S9*D*).

To overcome this, we first depleted MR1$^{\text{FOLDED}}$ from digitonin lysates with mAb 8F2.F9 and then used αMR1-CT to IP the remaining MR1 conformer (MR1$^{\text{OPEN}}$, 8G3 "reactive"). The absence of β_2m in the IP (Fig. 7*E*) demonstrated that this was indeed the retrieved MR1 conformer, and the presence of TPN confirmed the interaction between this chaperone and MR1$^{\text{OPEN}}$ (Fig. 7*E*). However, the TPN–MR1$^{\text{OPEN}}$ complex did not coprecipitate with TAP1, suggesting that unlike MR1$^{\text{FOLDED}}$, this conformer was not associated with the PLC. We could not determine whether TAPBPR also coprecipitated with MR1 in these experiments since it would be obscured by the presence of the HC of the antibodies used for IP. Given the additive effect of TAPBPR deletion over that of TPN alone on MR1 abundance (Fig. 7*A*) and half-life (Fig. 7*C*), and the in silico modeling predictions (*SI Appendix*, Figs. S6–S8), it is likely that TAPBPR can also contribute to MR1 stabilization, but we cannot tell if or to what extent this can happen in cells that express TPN. Regardless of this limitation, we can conclude that two conformers of unloaded MR1 molecules exist in the ER (*SI Appendix*, Fig. S9*E*): The first (MR1$^{\text{FOLDED}}$) is complexed with β_2m and bound to the PLC, whereas the second is not bound to β_2m or to the PLC but is stabilized by binding to TPN and, perhaps, TAPBPR. Furthermore, the association of MR1$^{\text{OPEN}}$ with TPN and TAPBPR may promote its transition to the MR1$^{\text{FOLDED}}$ conformation.

Discussion

The mechanism and location of exogenous VitBAg capture and presentation by MR1 has been unclear. Other antigen-presenting molecules, such as MHC class II and CD1a-d, migrate to endosomal compartments associated with endogenous ligands that are then replaced by endocytosed antigens. It was expected that MR1 might follow a similar mechanistic pathway for presentation of VitBAg. Indeed, before the discovery of MR1 ligands, studies had suggested that MR1 and MHC-II pathways likely overlap (20). However, we demonstrated that, in the absence of exogenous antigens, most MR1 molecules are retained in an empty state inside the ER (14), and indirect evidence suggested that this might be the location where MR1 binds VitBAg before trafficking to the cell surface (14, 46).

Here we were able to directly monitor MR1–ligand complex formation by designing a fluorophore-labeled MR1-binding ligand, MAgA-TAMRA, based on the structures of the most potent known MAIT cell antigen, 5-OP-RU (4), and its more chemically-stable analog, JYM72 (5). MAgA-TAMRA is a valuable tool for directly monitoring ligand interaction with MR1

in cells, that provided direct evidence here that extracellular ligands primarily bind to MR1 located in the ER. PLA showed that detectable MR1–MAgA-TAMRA complexes are formed inside the ER within 10 min after incubating cells with the ligand, and most of the complexes formed over 1 h leave the ER within the next 2 h. IP of MR1–MAgA-TAMRA complexes with antiserum against TAMRA showed that the small molecule ligand initially encounters MR1 present in the ER, with subsequent trafficking through the Golgi. The kinetics of MAgA-TAMRA uptake and elimination, and of MR1 presentation, were comparable to those for the natural ligand 5-OP-RU. Thus, our observations for MAgA-TAMRA are likely relevant to closely related native microbial antigens also captured by MR1 and presented to MAIT cells (10, 13). This conclusion leads to interesting possibilities for future therapeutic exploitation of the MR1 presentation pathway using analogs of its natural ligands. Despite chemical modifications to the natural antigen 5-OP-RU, the synthetic analog MAgA-TAMRA was still able to traffic to the ER, bind to MR1 molecules, and inhibit MAIT cell recognition of other ligands. MAgA-TAMRA helps to further define the structural limitations and ligand tolerance in the Ag binding cleft of MR1, which can accommodate a variety of small molecules (47), and it serves as a blueprint for creating new MR1 ligands customized with different payloads and functionalities for studying MR1 biology (5, 48, 49).

The ability of MR1-presenting cells to uptake and present extracellular VitBAg was recently shown to be critical for the selection and activation of MAIT cells in vivo (8, 13). Using MAgA-TAMRA, we can directly observe that MR1 captures such Ag inside the ER. In contrast, Ag derived from intracellular bacteria residing in endosomes or phagosomes may bind to MR1 in these post-ER compartments, as suggested by other studies (18–20). However, it cannot be discarded that such Ag may in fact traffic to the ER and then bind to MR1 in this location. The relative role of ligand loading in the ER vs. endosomal compartments in different scenarios of infection thus remains to be fully elucidated.

Although the mechanism of transport of extracellular or endosomal ligands into the ER is unknown, the reliance of VitBAg presentation on ER-resident MR1 highlights the importance of maintaining a pool of ligand-receptive MR1 molecules within this compartment. Our two unbiased screening approaches to discover proteins required for efficient MR1-antigen presentation revealed a role for the ER chaperone TPN in maintaining this pool, illustrated by the impact of TPN deletion on the presentation of MR1-VitBAg in the C1R cell line and in primary bronchial epithelial cells. Since MR1 could still present antigen in the absence of TPN, we speculated that the related chaperone TAPBPR may have a similar role. Deletion of TAPBPR alone did nothing but, in cooperation with TPN deletion, substantially reduced ER-resident MR1 through accelerating MR1 degradation. Thus, TPN and TAPBPR protect MR1 from degradation, most likely through the ER-associated degradation pathway (50). The impact of TPN/TAPBPR deficiency on VitBAg presentation was particularly noticeable when the concentration of the latter was limiting. Lack of TPN and TAPBPR did not affect the kinetics of egress, nor the half-life, of MR1–ligand complexes generated in the ER. Hence, the role of these chaperones is not to assist Ag loading but to stabilize and increase the half-life of the ligand-free ER pool of MR1 molecules, thus maintaining the number available for Ag presentation. To our knowledge, this study reporting a functional role for TPN and TAPBPR in MR1 biology, is unique.

To further characterize the ER-resident MR1 molecules, we produced mAb 8G3 that recognizes a cohort of "open" MR1 not bound to β_2m. Previous IP studies, employing the αMR1-CT rabbit serum raised against the MR1 cytosolic tail, appeared to pull down subequimolar amounts of β_2m, leading us to conclude that unliganded MR1 molecules are weakly associated with β_2m (14). Using 8G3 here we find that the ER contains two conformers of empty MR1, one devoid of β_2m (8G3-reactive) and the other forming MR1-β_2m dimers that were recognized by mAb 8F2.F9. The two MR1 conformers differentially associate with components of the PLC. Coprecipitation showed that the β_2m-free MR1 conformer was associated with TPN but, if it was also bound to other PLC members, this association was weak and was not maintained during IP with mAb 8G3. In contrast, MR1–β_2m dimers immunoprecipitated with 8F2.F9 pulled down all other components of the PLC. We cannot discount the possibility that some association only occurred when MR1 was overexpressed, but the endogenous level of MR1 is too low to perform reliable coprecipitation studies. TPN deletion did have an impact on the endogenous (low) MR1 expression level of primary NHBE cells and C1R and 721.220 cell lines that were not transfected with MR1, so the interactions we describe also apply to endogenous MR1. The fact that TAP deletion did not affect MR1 presentation of 5-OP-RU or MAgA-TAMRA suggests that association with the PLC is not essential for MR1 function, implying that TPN can also stabilize empty MR1–β_2m dimers without docking to TAP, as it appears to do with the β_2m-free MR1 conformer. We also coprecipitated MHC-I with MR1, suggesting that both molecules can coassociate in a hybrid PLC. This is plausible as it has been estimated that the PLC has two loading modules comprising two MHC-I molecules, each bound to the other components of the PLC, docking around a single TAP molecule (31). Previous studies that investigated interactions between the PLC and murine MR1 reached similar conclusions to our own. However, those studies were conducted before the discovery of the identities of MR1 ligands, and therefore could not measure the role of the PLC or other ER chaperones on MR1 antigen presentation, nor distinguish between a role in empty MR1 stabilization versus a role in ligand binding (8, 17, 23).

While MR1 association with chaperones also involved in MHC-I Ag presentation may appear unsurprising, given the similarity between MR1 and MHC-I, not all MHC-I–like molecules display such associations, such as the CD1 family (51) and the HFE protein (52), and not all MHC-I allomorphs are dependent on TPN. The empty MR1 conformers that bind TPN, TAPBPR, and the PLC are likely to be structurally closer to MHC-I than CD1s, at least in the regions involved in these interactions. This notion is supported by the observation that the same mutations that hamper TPN from binding to MHC-I also reduce its capacity to stabilize empty MR1. In silico modeling predicts that MR1 may interact with TPN and TAPBPR using a conserved binding mode like that established for MHC-I.

Here we have established that in order to efficiently bind and present soluble VitBAg, a large proportion of unloaded MR1 molecules are required to be maintained within the ER. We have shown that MR1 molecules bind to the same chaperones that stabilize empty MHC-I, namely TPN and possibly TAPBPR. MR1 was also found to be associated with the components of the PLC, however the loss of the PLC (by TAP1 deletion) did not affect MR1 presentation of VitBAg. Hence, the main functions of the PLC for MHC-I do not appear to be crucial for MR1 presentation: first, while TAP supplies peptide Ag to the ER lumen for MHC-I, it is not required to transport VitBAg into the ER; second, the PLC's editing function to select high-affinity Ag for MHC-I (53–55) does not seem to be required for MR1. MR1 uses a different "quality control" system to select suitable ligands, namely their capacity to form a Schiff base with the Lys43 of the MR1 antigen-binding site (3, 4). While some ligands are known to bind weakly to MR1 without forming a Schiff base, the resulting complexes are not efficiently transported to the cell surface (47) or are not potent activators of MAIT cells. Furthermore, while TPN or TAPBPR likely open the MR1

Ag-binding groove, it is only at the F′ pocket and not at the A′ pocket where VitBAg bind, hence their participation in VitBAg-exchange or editing is unlikely.

Our findings raise interesting possibilities that merit further investigation. First, HLA alleles may compete with MR1 for binding to TPN or the PLC, and pathologies that cause HLA down-regulation such as viral infection or cancer may free TPN/TAPBPR and result in greater MR1 ER stabilization, expression, and presentation. Second, structural features of TPN/TAPBPR may have evolved mainly not only to chaperone peptide presentation by MHC-I but also VitBAg presentation by MR1, or both. Addressing these possibilities could shed further light on mechanisms of MR1-mediated antigen presentation.

Materials and Methods

MR1 Ligands and MAgA-TAMRA Stability. MR1 ligands were added directly to the culture medium at the indicated concentrations. Stock solutions of Ac-6-FP (Schircks Laboratories), 5-OP-RU [synthesized in DMSO, as previously described (5)], and MAgA-TAMRA were stored in DMSO. Methylglyoxal (Sigma Aldrich) and 5-A-RU [synthesized as previously described (5)] were stored in water. To assess stability of MAgA-TAMRA (**8**), a solution (0.14 mg, 0.16 μmol) in PBS (3.2 mL, pH 7.4) was incubated at 37 °C. Aliquots (20 μL) were withdrawn at various time points and analyzed by LCMS (flow rate = 0.5 mL/min, gradient: 0% solvent B to 100% solvent B over 5 min). The fraction corresponding to MAgA-TAMRA (**8**) contained the ions *m/z* 437.5 $[M+2H]^{2+}$, 873.4 $[M+H]^{+}$, and 871.4 $[M-H]^{-}$. Relative compound concentrations were determined by measuring the area under the curve for the peak at *m/z* 437.5 corresponding to MAgA-TAMRA (**8**).

Flow Cytometry for Detection of Ligands and FRET. Flow cytometry was performed on an LSR Fortessa (BD Biosciences) to measure 5-OP-RU by excitation with 405-nm laser and 450/50 emission filter, MAgA-TAMRA by excitation with 561-nm laser and 585/15 emission filter, and FRET between MAgA-TAMRA and Alexa Fluor 647 by excitation with 561-nm laser and 670/30 emission filter.

CRISPR/Cas9 Genome-wide Screening. For genome-wide screening, the GeCKO V1 library was used (35) (a gift from Feng Zhang, Broad Institute, Cambridge, MA) to transduce 60 million C1R cells in triplicate. After 5 d, transductants were selected with 1 μg/mL puromycin for 6 d. Libraries were split into two 60 million pools (per replicate): 1) to enrich for $MR1^{LOW}$ cells and (2) for an "unsorted" reference library, which was maintained in culture during the experiment. For the latter, >60 million cells were treated with 0.5 μM 5-OP-RU for 4 h, then stained for MR1 using biotinylated mAb 26.5 followed by PE-conjugated streptavidin. $MR1^{LOW}$ cells were isolated by FACS by gating on the bottom 5% of the PE channel. These cells were expanded in culture for 7 d and then $MR1^{LOW}$ cells were sorted for a second time using the same method. DNA was isolated from each replicate using a QIAamp DNA Blood Maxi Kit according to the manufacturer's instructions. The sgRNAs in each replicate were amplified using the two-step PCR method described previously (35) using Hot Start Taq Polymerase (New England Biolabs); however, in the second PCR we incorporated the 8-bp barcode into the reverse as well as forward primer. Barcoded amplicons were pooled and purified using Nucleo Mag NGS beads (Macherey-Nagel), then sequenced using a NextSEq. 500 (Illumina). CRISPR/Cas9 library data processing and differential representation analysis was performed using an established bioinformatics pipeline (56). Negative binomial linear models of sgRNA count data incorporated blocking terms to account for any batch effects introduced by independent library infections. The sgRNAs considered to be significantly enriched in $MR1^{LOW}$-sorted samples relative to unsorted controls were those with a log(fold-change) >1.5 and $-\log_{10}(P \text{ value})$ >6.

Identification of MR1 Binding Partners by MS. Proteins coimmunoprecipitating with MR1–GFP compared to free GFP were prepared for MS analysis using the FASP protein digestion method (57). Peptides were analyzed by nanoflow HPLC coupled to an Impact II UHR-QqTOF mass spectrometer (Bruker), as described previously (58). Raw MS files were processed with MaxQuant (v1.6.6.0) for feature detection and protein identification. Extracted peak lists were searched against the UniProtKB/Swiss-Prot *Homo sapiens* database (March 2019) and a separate reverse decoy database to empirically assess the false-discovery rate (FDR). The "match between runs" option in MaxQuant was used to transfer identifications made between runs on the basis of matching precursors with high mass accuracy (59, 60). LFQ was selected, with a minimum ratio count of 2. PSM and protein identifications were filtered using a target-decoy approach at an FDR of 1%. Only unique and razor peptides were considered for quantification with intensity values present in at least two of three replicates per group. Statistical analysis was performed using LFQAnalyst (https://bioinformatics.erc.monash.edu/apps/LFQ-Analyst/), whereby the LFQ intensity values were used for protein quantification. Missing values were replaced by values drawn from a normal distribution of 1.8 SDs and a width of 0.3 for each sample (Perseus-type). Protein-wise linear models combined with empirical Bayes statistics were used for differential expression analysis using Bioconductor package Limma, whereby the adjusted *P* value cutoff was set at 0.05 and $\log_2$ fold-change cutoff set at 1. The Benjamini–Hochberg method of FDR correction was used. The MS proteomics data have been deposited to the ProteomeXchange Consortium via the PRIDE (61) partner repository with the dataset identifier PXD014585 (62).

Statistical Analysis. Statistical analysis was performed using GraphPad Prism (v8.4.0). Comparisons between two groups were made using a *t* test, and paired *t* test with data from multiple experiments. Comparisons of more than two groups were made using one-way ANOVA for one parameter, or two-way for multiparameter, with repeated measures for data from multiple experiments. Each was followed by a multiple comparison test. The following *P* values were considered statistically significant: $*P < 0.05$, $**P < 0.01$, $***P < 0.001$, and $****P < 0.0001$.

Data Availability. Proteomics data have been deposited in the ProteomeXchange Consortium (accession no. PXD014585).

ACKNOWLEDGMENTS. We thank Dr. Louise Boyle (University of Cambridge) for the kind gift of the plasmids for TAPBPR expression and PeTe4 mAb; Prof. Peter Cresswell for the kind gift of the 148.3 and PaSta1 mAbs; and the Antibody Services Facility and Genomics Hub (Walter and Eliza Hall Institute) and the Melbourne Cytometry Platform from the Doherty Institute node and the Biological Optical Microscopy Platform (University of Melbourne) for expert assistance. H.E.G.M. is supported by an Australian Research Council (ARC) Discovery Early Career Researcher Award (DE170100575), a University of Melbourne Early Career Researcher Grant, and the AMP Tomorrow Fund; A.J.C. is supported by an ARC Future Fellowship (FT160100083); S.B.G.E. is supported by an ARC Discovery Early Career Researcher Award (DE170100407); J.R. is supported by an ARC Australian Laureate Fellowship; D.P.F. and J.A.V. are supported by National Health and Medical Research Council Research Fellowships (1117017, 1058193). This research was supported by a National Health and Medical Research Council Program Grant (1113293), an ARC Discovery Grant (170102471), and an ARC Centre of Excellence in Advanced Molecular Imaging Grant (CE140100011).

1. D. I. Godfrey, A. P. Uldrich, J. McCluskey, J. Rossjohn, D. B. Moody, The burgeoning family of unconventional T cells. *Nat. Immunol.* **16**, 1114–1123 (2015).
2. H. E. McWilliam, R. W. Birkinshaw, J. A. Villadangos, J. McCluskey, J. Rossjohn, MR1 presentation of vitamin B-based metabolite ligands. *Curr. Opin. Immunol.* **34**, 28–34 (2015).
3. L. Kjer-Nielsen *et al*., MR1 presents microbial vitamin B metabolites to MAIT cells. *Nature* **491**, 717–723 (2012).
4. A. J. Corbett *et al*., T-cell activation by transitory neo-antigens derived from distinct microbial pathways. *Nature* **509**, 361–365 (2014).
5. J. Y. Mak *et al*., Stabilizing short-lived Schiff base derivatives of 5-aminouracils that activate mucosal-associated invariant T cells. *Nat. Commun.* **8**, 14599 (2017).
6. H. Wang *et al*., Dual-targeting small-molecule inhibitors of the Staphylococcus aureus FMN riboswitch disrupt riboflavin homeostasis in an infectious setting. *Cell Chem. Biol.* **24**, 576–588.e6 (2017).
7. H. E. G. McWilliam, J. A. Villadangos, How MR1 presents a pathogen metabolic signature to mucosal-associated invariant T (MAIT) cells. *Trends Immunol.* **38**, 679–689 (2017).
8. E. Treiner *et al*., Selection of evolutionarily conserved mucosal-associated invariant T cells by MR1. *Nature* **422**, 164–169 (2003).
9. R. W. Birkinshaw, L. Kjer-Nielsen, S. B. G. Eckle, J. McCluskey, J. Rossjohn, MAITs, MR1 and vitamin B metabolites. *Curr. Opin. Immunol.* **26**, 7–13 (2014).
10. M. G. Constantinides *et al*., MAIT cells are imprinted by the microbiota in early life and promote tissue repair. *Science* **366**, eaax6624 (2019).
11. M. D. Crowther *et al*., Genome-wide CRISPR-Cas9 screening reveals ubiquitous T cell cancer targeting via the monomorphic MHC class I-related protein MR1. *Nat. Immunol.* **21**, 178–185 (2020).
12. M. Lepore *et al*., Functionally diverse human T cells recognize non-microbial antigens presented by MR1. *eLife* **6**, e24476 (2017).
13. F. Legoux *et al*., Microbial metabolites control the thymic development of mucosal-associated invariant T cells. *Science* **366**, 494–499 (2019).
14. H. E. McWilliam *et al*., The intracellular pathway for the presentation of vitamin B-related antigens by the antigen-presenting molecule MR1. *Nat. Immunol.* **17**, 531–537 (2016).

15. B. Abós *et al*., Human MR1 expression on the cell surface is acid sensitive, proteasome independent and increases after culturing at 26°C. *Biochem. Biophys. Res. Commun.* **411**, 632–636 (2011).
16. H. Yamaguchi, K. Hashimoto, Association of MR1 protein, an MHC class I-related molecule, with β(2)-microglobulin. *Biochem. Biophys. Res. Commun.* **290**, 722–729 (2002).
17. M. J. Miley *et al*., Biochemical features of the MHC-related protein 1 consistent with an immunological function. *J. Immunol.* **170**, 6090–6098 (2003).
18. M. J. Harriff *et al*., Endosomal MR1 trafficking plays a key role in presentation of Mycobacterium tuberculosis ligands to MAIT cells. *PLoS Pathog.* **12**, e1005524 (2016).
19. E. Karamooz, M. J. Harriff, G. A. Narayanan, A. Worley, D. M. Lewinsohn, MR1 recycling and blockade of endosomal trafficking reveal distinguishable antigen presentation pathways between Mycobacterium tuberculosis infection and exogenously delivered antigens. *Sci. Rep.* **9**, 4797 (2019).
20. S. Huang *et al*., MR1 uses an endocytic pathway to activate mucosal-associated invariant T cells. *J. Exp. Med.* **205**, 1201–1211 (2008).
21. O. Patel *et al*., Recognition of vitamin B metabolites by mucosal-associated invariant T cells. *Nat. Commun.* **4**, 2142 (2013).
22. S. B. Eckle *et al*., A molecular basis underpinning the T cell receptor heterogeneity of mucosal-associated invariant T cells. *J. Exp. Med.* **211**, 1585–1600 (2014).
23. F. Tilloy *et al*., An invariant T cell receptor alpha chain defines a novel TAP-independent major histocompatibility complex class Ib-restricted alpha/beta T cell subpopulation in mammals. *J. Exp. Med.* **189**, 1907–1921 (1999).
24. M. Gullberg, A.-C. Andersson, Visualization and quantification of protein-protein interactions in cells and tissues. *Nat. Methods* **7**, 480 (2010).
25. W. J. Chua *et al*., Endogenous MHC-related protein 1 is transiently expressed on the plasma membrane in a conformation that activates mucosal-associated invariant T cells. *J. Immunol.* **186**, 4744–4750 (2011).
26. S. Huang *et al*., Evidence for MR1 antigen presentation to mucosal-associated invariant T cells. *J. Biol. Chem.* **280**, 21183–21193 (2005).
27. N. J. Stam, H. Spits, H. L. Ploegh, Monoclonal antibodies raised against denatured HLA-B locus heavy chains permit biochemical characterization of certain HLA-C locus products. *J. Immunol.* **137**, 2299–2306 (1986).
28. F. Perosa *et al*., Beta 2-microglobulin-free HLA class I heavy chain epitope mimicry by monoclonal antibody HC-10-specific peptide. *J. Immunol.* **171**, 1918–1926 (2003).
29. M. F. Sernee, H. L. Ploegh, D. J. Schust, Why certain antibodies cross-react with HLA-A and HLA-G: Epitope mapping of two common MHC class I reagents. *Mol. Immunol.* **35**, 177–188 (1998).
30. W. Zhang, P. A. Wearsch, Y. Zhu, R. M. Leonhardt, P. Cresswell, A role for UDP-glucose glycoprotein glucosyltransferase in expression and quality control of MHC class I molecules. *Proc. Natl. Acad. Sci. U.S.A.* **108**, 4956–4961 (2011).
31. A. Blees *et al*., Structure of the human MHC-I peptide-loading complex. *Nature* **551**, 525–528 (2017).
32. R. Battle, K. Poole, S. Haywood-Small, B. Clark, M. N. Woodroofe, Molecular characterisation of the monocytic cell line THP-1 demonstrates a discrepancy with the documented HLA type. *Int. J. Cancer* **132**, 246–247 (2013).
33. L. H. Boyle *et al*., Tapasin-related protein TAPBPR is an additional component of the MHC class I presentation pathway. *Proc. Natl. Acad. Sci. U.S.A.* **110**, 3465–3470 (2013).
34. C. Hermann *et al*., TAPBPR alters MHC class I peptide presentation by functioning as a peptide exchange catalyst. *eLife* **4**, e09617 (2015).
35. O. Shalem *et al*., Genome-scale CRISPR-Cas9 knockout screening in human cells. *Science* **343**, 84–87 (2014).
36. B. Ortmann *et al*., A critical role for tapasin in the assembly and function of multimeric MHC class I-TAP complexes. *Science* **277**, 1306–1309 (1997).
37. Y. Shimizu, R. DeMars, Production of human cells expressing individual transferred HLA-A,-B,-C genes using an HLA-A,-B,-C null human cell line. *J. Immunol.* **142**, 3320–3328 (1989).
38. B. Sadasivan, P. J. Lehner, B. Ortmann, T. Spies, P. Cresswell, Roles for calreticulin and a novel glycoprotein, tapasin, in the interaction of MHC class I molecules with TAP. *Immunity* **5**, 103–114 (1996).
39. D. Zernich *et al*., Natural HLA class I polymorphism controls the pathway of antigen presentation and susceptibility to viral evasion. *J. Exp. Med.* **200**, 13–24 (2004).
40. B. Gao *et al*., Assembly and antigen-presenting function of MHC class I molecules in cells lacking the ER chaperone calreticulin. *Immunity* **16**, 99–109 (2002).
41. D. R. Peaper, P. Cresswell, Regulation of MHC class I assembly and peptide binding. *Annu. Rev. Cell Dev. Biol.* **24**, 343–368 (2008).
42. C. Hermann, L. M. Strittmatter, J. E. Deane, L. H. Boyle, The binding of TAPBPR and Tapasin to MHC class I is mutually exclusive. *J. Immunol.* **191**, 5743–5750 (2013).
43. G. Dong, P. A. Wearsch, D. R. Peaper, P. Cresswell, K. M. Reinisch, Insights into MHC class I peptide loading from the structure of the tapasin-ERp57 thiol oxidoreductase heterodimer. *Immunity* **30**, 21–32 (2009).
44. A. Neerincx *et al*., TAPBPR bridges UDP-glucose:glycoprotein glucosyltransferase 1 onto MHC class I to provide quality control in the antigen presentation pathway. *eLife* **6**, e23049 (2017).
45. C. Thomas, R. Tampé, Structure of the TAPBPR-MHC I complex defines the mechanism of peptide loading and editing. *Science* **358**, 1060–1064 (2017).
46. M. Salio *et al*., Ligand-dependent downregulation of MR1 cell surface expression. *Proc. Natl. Acad. Sci. U.S.A.* **117**, 10465–10475 (2020).
47. A. N. Keller *et al*., Drugs and drug-like molecules can modulate the function of mucosal-associated invariant T cells. *Nat. Immunol.* **18**, 402–411 (2017).
48. W. Awad *et al*., The molecular basis underpinning the potency and specificity of MAIT cell antigens. *Nat. Immunol.* **21**, 400–411 (2020).
49. G. J. M. Ler *et al*., Computer modelling and synthesis of deoxy and monohydroxy analogues of a ribitylaminouracil bacterial metabolite that potently activates human T cells. *Chemistry* **25**, 15594–15608 (2019).
50. K. Römisch, Endoplasmic reticulum-associated degradation. *Annu. Rev. Cell Dev. Biol.* **21**, 435–456 (2005).
51. M. Sugita, P. J. Peters, M. B. Brenner, Pathways for lipid antigen presentation by CD1 molecules: Nowhere for intracellular pathogens to hide. *Traffic* **1**, 295–300 (2000).
52. S. M. Rizvi, M. Raghavan, Direct peptide-regulatable interactions between MHC class I molecules and tapasin. *Proc. Natl. Acad. Sci. U.S.A.* **103**, 18220–18225 (2006).
53. M. J. Barnden, A. W. Purcell, J. J. Gorman, J. McCluskey, Tapasin-mediated retention and optimization of peptide ligands during the assembly of class I molecules. *J. Immunol.* **165**, 322–330 (2000).
54. G. Fleischmann *et al*., Mechanistic basis for epitope proofreading in the peptide-loading complex. *J. Immunol.* **195**, 4503–4513 (2015).
55. C. Thomas, R. Tampé, Proofreading of peptide-MHC complexes through dynamic multivalent interactions. *Front. Immunol.* **8**, 65 (2017).
56. Z. Dai *et al*., edgeR: A versatile tool for the analysis of shRNA-seq and CRISPR-Cas9 genetic screens. *F1000 Res.* **3**, 95 (2014).
57. J. R. Wiśniewski, A. Zougman, N. Nagaraj, M. Mann, Universal sample preparation method for proteome analysis. *Nat. Methods* **6**, 359–362 (2009).
58. L. F. Dagley, G. Infusini, R. H. Larsen, J. J. Sandow, A. I. Webb, Universal solid-phase protein preparation (USP^3) for bottom-up and top-down proteomics. *J. Proteome Res.* **18**, 2915–2924 (2019).
59. J. Cox *et al*., Accurate proteome-wide label-free quantification by delayed normalization and maximal peptide ratio extraction, termed MaxLFQ. *Mol. Cell. Proteomics* **13**, 2513–2526 (2014).
60. J. Cox, M. Mann, MaxQuant enables high peptide identification rates, individualized p.p.b.-range mass accuracies and proteome-wide protein quantification. *Nat. Biotechnol.* **26**, 1367–1372 (2008).
61. Y. Perez-Riverol *et al*., The PRIDE database and related tools and resources in 2019: Improving support for quantification data. *Nucleic Acids Res.* **47**, D442–D450 (2019).
62. L. F. Dagley, H. E. G. McWilliam, Endoplasmic reticulum chaperones stabilize ligand-receptive MR1 molecules for efficient presentation of metabolite antigens. PRIDE. https://www.ebi.ac.uk/pride/archive/projects/PXD014585. Deposited 7 December 2019.